Available online at www.sciencedirect.com
SCIENCE DIRECT
Polymer 46 (2005) 11969–11977
polymer
www.elsevier.com/locate/polymer

Nanoindentation and morphological studies on injection-molded nylon-6 nanocomposites

Lu Shen [a], Wuiwui Chauhari Tjiu [a], Tianxi Liu [b,*]

[a] *Institute of Materials Research and Engineering, 3 Research Link, Singapore 117602, Singapore*
[b] *Laboratory of Advanced Materials, Fudan University, 220 Handan Road, Shanghai 200433, People's Republic of China*

Received 11 April 2005; received in revised form 18 August 2005; accepted 3 October 2005
Available online 26 October 2005

Abstract

The nanoindentation behavior and morphology of the injection-molded specimens of nylon-6 (PA6)/clay nanocomposites prepared by melt-compounding have been studied in present study. The elastic and plastic properties as well as creep behavior of PA6 and its nanocomposites are comparatively evaluated as the function of clay loading by using nanoindentation technique. The anisotropic characteristics in mechanical properties are studied by indenting the injection-molded specimens in two different directions (i.e. parallel and perpendicular to the injection direction). The uneven distribution of both the clay nanofiller and the crystallinity of the polymeric matrix induced by melt-processing leads to the variation of the mechanical property of the nanocomposites in certain directions and locations within the molded specimens. The microstructural and morphological changes of PA6 upon incorporating with clay nanofiller are evidenced by transmission electron microscopy and small-angle X-ray scattering, which are closely correlated with the anisotropy of the mechanical properties observed by nanoindentation.

Keywords: Nylon-6; Nanocomposites; Nanoindentation

1. Introduction

In the past decade, polymer nanocomposites have attracted much interest in both academic and industrial arenas because of their enhanced physical properties, including tensile strength, modulus, heat distortion temperature, fire retardancy and gas permeability [1–3]. In the family of polymer nanocomposites, clay-based nanocomposites have received a great deal of attention because of the high aspect ratio of nanoclay platelets and their fine dispersion within the polymeric matrices to form intercalation/exfoliation reinforcement mechanisms [4,5]. In the late 1980s, the researchers from Toyota successfully developed nylon-6 (PA6)/organophilic montmorillonite clay nanocomposites by in situ polymerization [1,6,7]. They reported that the PA6/clay nanocomposites exhibit superior tensile strength, tensile modulus, flexural strength, heat distortion temperature, water and gas barrier properties and with comparable impact strength as neat PA6 [8–13]. Generally, the preparation methods of polymer/clay nanocomposites are mainly divided into three groups according to the starting materials and processing techniques: intercalation of polymer or pre-polymer from solution, in situ intercalative polymerization method, and melt intercalation method [4]. The melt intercalation method is widely used to develop polymer/clay nanocomposites because it has more advantages than either in situ intercalative polymerization or polymer solution intercalation. First, it is environmentally benign due to the absence of organic solvents. Second, it is compatible with conventional industrial processes, such as extrusion and injection and other polymer processing techniques, thus being easily commercialized. And, the melt intercalation method may allow the use of polymers which are previously not suitable for in situ polymerization or solution intercalation [4].

In the process of melt intercalation, the rheological and thermodynamic character of the materials can be important as it may affect the degree of exfoliation and the dispersion of nanofillers. In a recent study, we have presented the inhomogeneous distribution of both the well-dispersed clay and the crystalline structures in PA6 matrix due to polymer melt processing [14]. This kind of processing-induced pattern of material morphologies is expected to cause the variation or distribution of (local) mechanical properties inside the specimens, thus affect the performance of the final products [15–17].

* Corresponding author. Tel.: +86 21 556 64197; fax: +86 21 556 64192.
E-mail address: txliu@fudan.edu.cn (T. Liu).

0032-3861/$ - see front matter © 2005 Elsevier Ltd. All rights reserved.
doi:10.1016/j.polymer.2005.10.006

Balta Calleja [18–22] and other researchers [23] have extensively studied the structure-property relationship of the polymers by microindentation technique. This advanced technique can provide a wealth of valuable quantitative information on the mechanical properties of the sample surfaces depending on the localized deformation [24–27]. The dimension of the deformation is in the magnitude of micron level. It is, therefore, possible to correlate the mechanical characteristics with certain microstructures in the materials. In addition, the morphologically anisotropic materials in different loading directions or under certain pre-deformed situation could be evaluated by the indentation technique as well [22].

In an indentation experiment, the yield stress is normally exceeded and the indentation depth variation is a combination of both viscoelastic and viscoplastic contributions to the total indentation depth. This technique has been applied on polymeric bulk materials [28–30] as well as thin films [31,32] to characterize the mechanical properties at the near-surface and interface areas. To our knowledge, few studies on the hardness and modulus along different directions in the injection-molded polymer/clay nanocomposites have been carried out. In present study, the nanoindentation technique is used to study the anisotropy characteristics of mechanical properties of the injectionmolded PA6/clay nanocomposites. The elastic and plastic properties as well as creep behavior of neat PA6 and its nanocomposites have been comparatively evaluated as a function of clay loading. An attempt has been made to correlate the observed mechanical properties with the morphological changes due to the addition of nanoclay and the injection process.

2. Experimental

2.1. Materials and sample preparation

The PA6 pellets (Grade SF® 1080A) used in this study were provided by Ube Industries (under license from Toyota). The organically modified clay (Nanomer® I.30TC) was supplied by Nanocor Inc. All of the materials were dried in a vacuum oven at 80 °C for 24 h prior to use. A wide range of PA6/clay nanocomposites containing 0, 1.25, 2.5, 5, 7.5 and 10 wt% clay was prepared via a melt-compounding method using a Brabender twin-screw extruder at 250 °C with a screw speed of 80 rpm [14]. The extruded nanocomposite pellets were fabricated into rectangular specimens (with dimension of $6.5\times 12.7\times 150\ mm^3$) by using an injection molding machine (Battenfeld 300 CD plus). The barrel temperature was set at 250 °C and the mold temperature at 80 °C.

2.2. Transmission electron microscopy

The morphologies of the PA6/clay nanocomposites were studied by using a Philips CM300-FEG transmission electron microscope (TEM) under an accelerating voltage of 200 kV. Thin sections (with thickness of about 70 nm) for TEM observations were cut from the cross-section of the injection-molded bars under cryogenic conditions by using a Leica ultramicrotome with a diamond knife.

2.3. Small-angle X-ray scattering (SAXS) measurements

SAXS experiments were performed on a small-angle diffractometer (Bruke Nanostar), using Cu $K_{\alpha 1}$ radiation source ($\lambda=0.15418$ nm). The SAXS data were corrected for absorption, background scattering and the fluctuation of incident beam intensity, followed by smoothing of the data, using the procedures described previously [33]. The one-dimensional correlation function was calculated by using the approach developed by Strobl et al. [34,35]. The long period (L) can be obtained from the maximum peak of the corrected Lorentz curves using Bragg law. The lamellar thickness (l_c) is approximately estimated by using $l_c=LW_c$; W_c is the degree of crystallinity which can be obtained by calorimetry or X-ray scattering [14].

2.4. Nanoindentation testing

The nanoindentation technique was employed to study the material's hardness, modulus, creep behavior and anisotropy of mechanical properties induced by injection molding process. Fig. 1 schematically shows an injection-molded specimen. Two sets of experiments were performed on the samples for different purposes. Firstly, to study the clay loading effect on the indentation behavior, PA6 samples with 0, 2.5, 5, 7.5 and 10 wt% of clay were indented on surface A. The indentation direction is perpendicular to the injection direction (indicated by arrow). Secondly, to study the anisotropic character of mechanical property of PA6 and its nanocomposites, the neat PA6 and two nanocomposite samples containing 5 and 10 wt% clay were cut and polished to expose three surfaces, i.e. A, B, and C (as shown in Fig. 1), for the subsequent nanoindentation experiments. The indentation tests were performed using an UMIS-2000H Nanoindentation system (Australian Scientific Instruments) with a Berkovich indenter (three-faced pyramid diamond). The load and depth of penetration were independently measured by two LVDT (linear variable differential transformer) sensors. From the experimentally determined load-penetration data, the hardness (H) and the elastic modulus

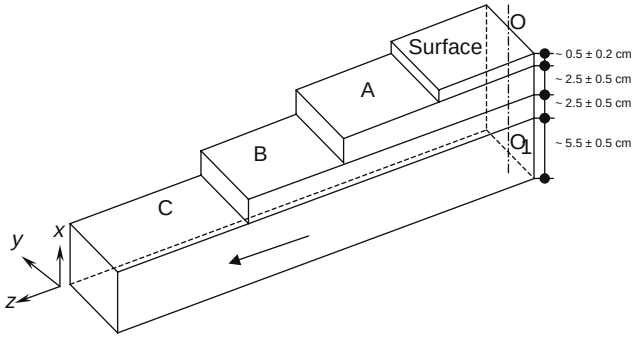

Fig. 1. Illustration of an injection-molded bar and three surface regions (A, B and C) for indentation measurements. The arrow indicates injection flow direction.

(E) were determined through the following analysis:

$$H = \frac{P_{\max}}{A} \tag{1}$$

$$\frac{E}{1-\nu^2} = \frac{\sqrt{\pi}}{2}\frac{1}{\sqrt{A}}\frac{\mathrm{d}P}{\mathrm{d}h} \tag{2}$$

where the hardness of the specimen can be defined as the average pressure that the specimen can withstand under a sharp indenter; $P_{\max}$ is indentation maximum load; A is the contact area at the maximum load; ν is Poisson's ratio ($\nu = 0.35$ for current study [21]); $\mathrm{d}P/\mathrm{d}h$ is the unloading stiffness, represented by the initial slope of the unloading curve. The area of the indentation is related to the depth of penetration, and for an ideal sharp Berkovich indenter, there is the following relation [24]:

$$A = 24.56h^2 \tag{3}$$

The indentation procedure performed on all samples was as follows. Firstly, the indenter was brought into contact with the sample surface at a constant strain rate (0.05 s^{-1} in present study) until the load achieved 40 mN. The load was held at the maximum value for 60 s to determine the creep behavior. The indenter was then withdrawn from the sample surface in the same rate until 2% of the maximum load was reached. Since, the polymeric materials have prominent strain-hardening effect [36], the constant strain rate was used to control the load applying on the samples. A minimum of 10 indents was made in each individual test. The averaged hardness and modulus values were obtained from the unloading curve by Oliver and Pharr method [24].

3. Results and discussion

3.1. Effect of nanoclay loading on modulus and hardness of PA6 matrix

The averaged load-displacement relations of neat PA6 and its nanocomposites with different clay loadings are illustrated in Fig. 2. It is clearly shown that the maximum depth for the five samples monotonously decreases with increasing clay concentration. According to Eq. (3), the larger displacement (h) corresponds to larger contact area (A) for a specified indenter. In present experiments, the applied maximum load is maintained at 40 mN. Therefore, the hardness is proportional to the reciprocal of the contact area (Eq. (1)). The result indicates that clay addition enhances the polymer's hardness with increasing the clay concentration. On the other hand, it is also noted that the initial unloading gradients of the five samples increase with clay concentration in the nanocomposites. It is known from Eq. (2) that the modulus is determined by the initial gradient of the unloading curve, which corresponds to the unloading stiffness ($\mathrm{d}P/\mathrm{d}h$), together with the contact area (A). As a result, the modulus of the nanocomposite changes with the clay loading as well. The creep behavior of the samples is represented in the maximum holding session where the materials are subjected to same load condition, i.e. 40 mN for 60 s. It is found that the amount of the creep displacement at the maximum holding section consistently decreases with clay loading. The detailed discussion on the creep behavior of the nanocomposites is to be given in following section.

It is noticed that the 5 wt% specimen showed very distinct load-displacement relation comparing with those with 2.5 and 7.5 wt% of clay. It is believed to be the overall outcome of the elastic–plastic response from the composite due addition of clay. The averaged plastic response (hardness) and the elastic response (modulus) for neat PA6 and its nanocomposites are summarized in Fig. 3. The hardness and modulus are shown to increase steadily with the clay loading as expected. With addition of only 2.5 wt% of clay, the modulus of the polymer has improved by about 74%, from 1.06 to 1.84 GPa, as compared with its neat counterpart; while with addition of 10 wt% of clay, the modulus is enhanced by approximately 128%. In addition, it is found that the pace of increment in modulus has been slowing down by further increasing the clay concentration from 2.5 to 10 wt%. This may be related to the clay morphology within the matrix. From our previous work, the morphology of clay dispersion in PA6 matrix is changed from exfoliation-dominated to intercalation/exfoliation

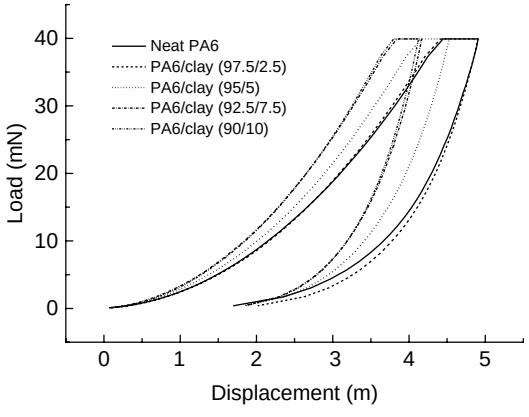

Fig. 2. Typical indentation load versus displacement curves of PA6 and its nanocomposites as a function of clay loading.

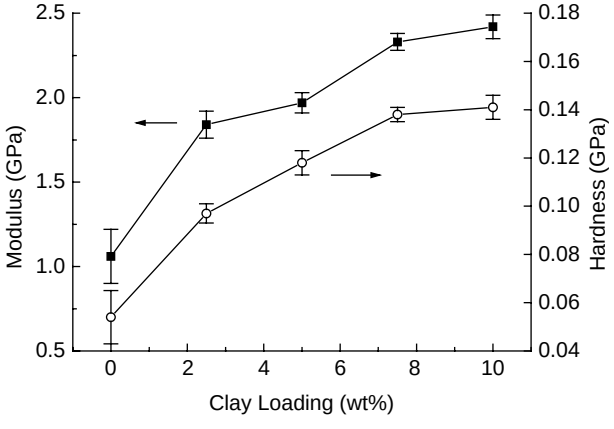

Fig. 3. Moduli and hardness of PA6 and its nanocomposites as a function of clay loading.

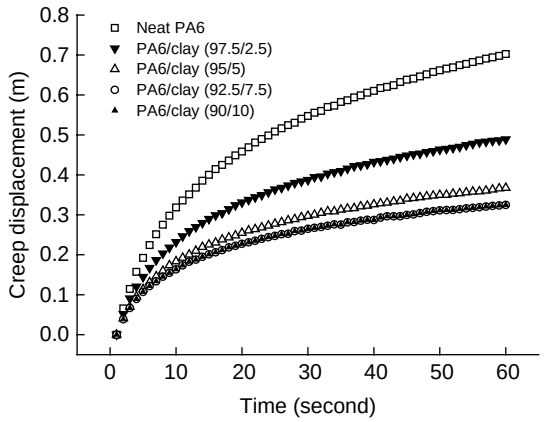

Fig. 4. Creep behaviors of PA6 and its nanocomposites as a function of clay loading.

mixture when clay loading exceeds 5 wt%, as evidenced by TEM and XRD [14]. It has been well documented that the intercalated clay morphology offers less enhancement in mechanical strength than the exfoliated one [4,14,37,38]. Thus, it is not surprising to find the above changing trend of the modulus with increasing clay loading. Similar phenomenon is also found in hardness profile. The hardness has improved by about 161% from 0.054 GPa for the neat PA6 to 0.141 GPa for the nanocomposite with 10 wt% of clay.

3.2. Creep behavior and morphology

Fig. 4 compares the creep displacements of neat PA6 and its nanocomposites, which are deformed under constant load of 40 mN for 60 s. The *y*-axis represents the relative displacement incurred in the course of holding process. It can be seen that the neat sample shows the maximum creep susceptibility and the greatest creep rate, compared with those of the nanocomposites. For the nanocomposite with 2.5 wt% of clay, its creep displacement in 60 s is reduced by about 30% compared with the neat system. The addition of rigid clay nanofiller is believed to be the cause of the enhancement of the creep resistance of the nanocomposites. Moreover, it is interesting to note that the creep resistance of the nanocomposites does not monotonously increase with clay loading. At higher clay loadings, i.e. 7.5 and 10 wt%, it is difficult to differentiate the creep behavior of the two nanocomposite samples. This unexpected phenomenon may indicate that, in addition to the reinforcing effect from the nanoclay, there might be other opposite effects, which deteriorate the creep resistance of the nanocomposites (at higher clay concentrations). One of the main opposite effects is ascribed to the microstructural changes of PA6 matrix upon addition of clay nanofiller, as discussed below.

The morphological changes of PA6 due to addition of clay are investigated by TEM and SAXS. Fig. 5(A) shows the crystalline morphology of neat PA6 thin section microtomed from the molded specimen. A number of typical spherulites are observed with size of about 5 μm. Careful examination reveals that the well-developed spherulites consist of numerous closely

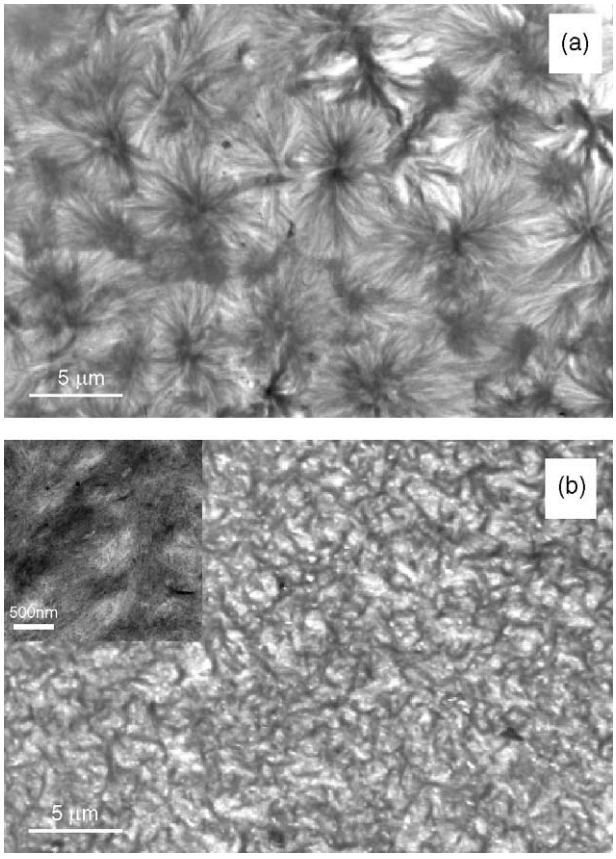

Fig. 5. TEM images showing crystalline morphologies of neat PA6 (A) and the nanocomposite with 2.5 wt% of clay (B). The insert is under high magnification.

stacked fibrillar lamellae which radically grow outward from the central regions (i.e. the nuclei). Upon incorporating nanoclay (e.g. 2.5 wt%) into the PA6 matrix, however, the crystalline texture of the matrix is greatly blurred, as shown in Fig. 5(B). The crystal size decreases significantly, and the well-defined spherulites are absent due to high (heterogeneous) nucleation density from clay nanofiller. And, only numerous bundle-like dark regions are observed with certain contrast. At higher magnification (the insert of Fig. 5(B)), these blurred crystalline bundles consisting of closely stacked lamellae can still be seen clearly. Close inspection also shows the presence of nanoclay platelets (darker lines in the insert). The microstructural changes with increasing clay concentration are further confirmed by SAXS measurements. Fig. 6 shows the Is^2 versus s curves (I is scattering intensity; s is the scattering vector, $s = 2 \sin \theta/\lambda$) for the nanocomposites as a function of clay content. It can be seen from the insert that the long period and the lamellar thickness are significantly reduced with increasing the loading level of clay nanofiller, as observed by other researchers in the same system [39–41].

Fig. 7 shows the effect of clay concentration on the crystallinity of PA6 nanocomposites. The degrees of crystallinity, $W_{c,XRD}$ and $W_{c,DSC}$, are calculated on the basis of previous X-ray diffraction (XRD) and differential scanning calorimetry (DSC) measurements, respectively [14]. It can be

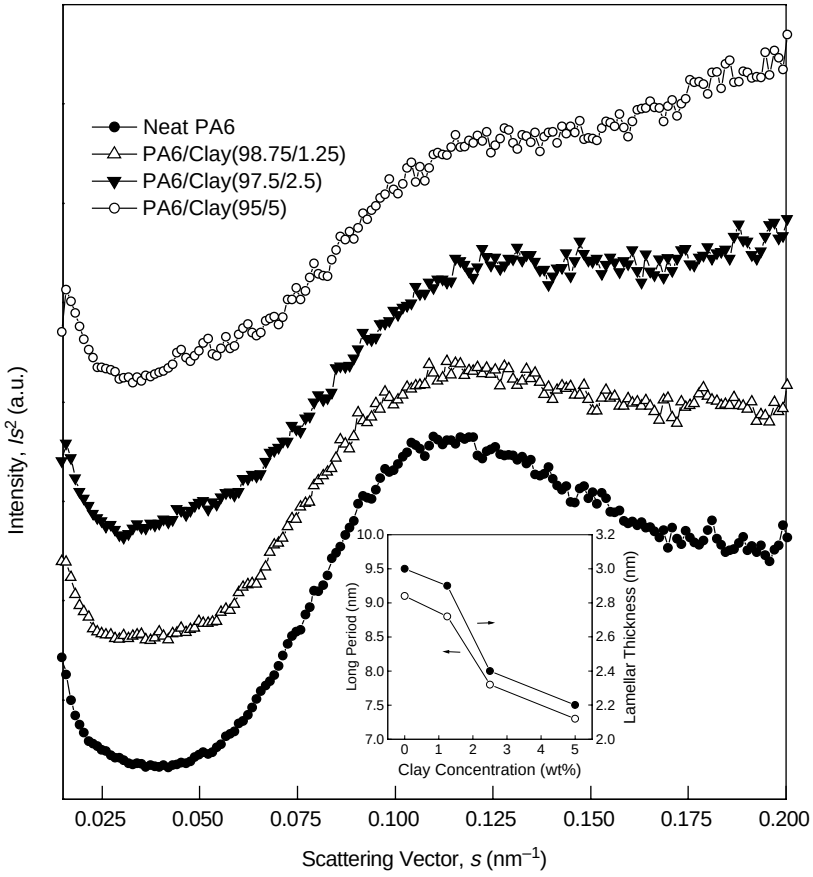

Fig. 6. Lorentz-corrected SAXS curves of Is^2 versus scattering vector s for the samples as a function of clay concentration. The insert shows the changes of long period and lamellar thickness with clay concentration.

seen that, despite of the difference in absolute values obtained by XRD and DSC methods, both of $W_{c,XRD}$ and $W_{c,DSC}$ decrease by about 30% with increasing clay loading up to 10 wt%. Therefore, it can be seen that the addition of nanoclay significantly reduces the crystal size and the degree of crystallinity of PA6 matrix, as also observed previously in nylon-66 nanocomposites [42,43]. Thus, it is believed that the dramatic changes of microstructure (e.g. the decreased crystal size and the reduced crystallinity) with increasing clay content are most probably contributed to the deterioration of creep resistance for the materials studied here, especially at higher clay loading. The two competing factors (i.e. enhancing effect from rigid nanoclay and deteriorating effect from change of crystalline morphology) simultaneously affect the creep behavior of the nanocomposites with increasing clay loading. From the present study, there exists a critical filler loading for the creep behavior of the nanocomposites, that is, 7.5 wt%: when nanoclay concentration is lower than 7.5 wt%, the reinforcing effect from rigid clay dominates; and when clay content is higher than 7.5 wt%, the microstructural changes of PA6 matrix due to the presence of clay play an important role. Similar phenomenon was also found in poly(ethylene oxide)/clay nanocomposites [23], where the critical value of nanofiller loading (for an adverse effect on the creep behavior) was found to be 5 wt%.

3.3. Anisotropic characteristics of mechanical property by nanoindentation

Fig. 8(A) shows the exfoliated clay morphology taken from the central region of an injection-molded nanocomposite specimen with 5 wt% clay. In addition, the TEM image clearly shows clay orientation (along the injection flow direction

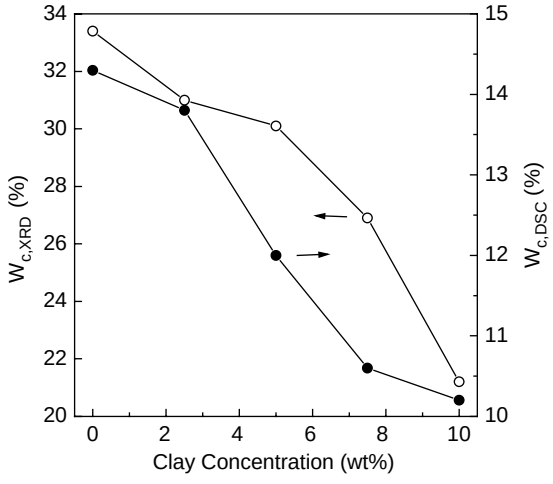

Fig. 7. Effect of clay content on the crystallinity of PA6 nanocomposites.

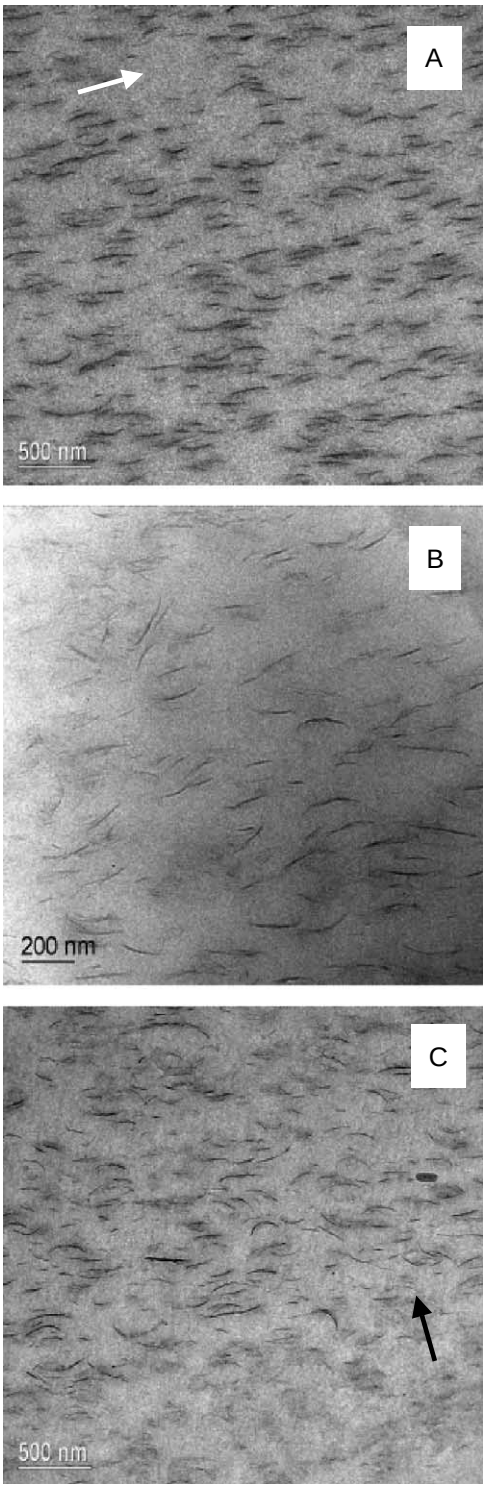

Fig. 8. (A) TEM images showing processing-induced clay orientation (within the center region of the molded specimen). The melt-processing direction is indicated by arrow. (B) TEM image at higher magnification showing well-exfoliated clay morphology. (C) TEM images showing inhomogeneous clay distribution from the near surface region to center (arrow direction) of the molded specimen.

indicated by arrow) induced by melt-processing. At higher magnification under TEM (Fig. 8(B)), the wellexfoliated clay nanoplatelets were clearly observed. Fig. 8(C) shows the clay distribution pattern in the nanocomposite by TEM taken from

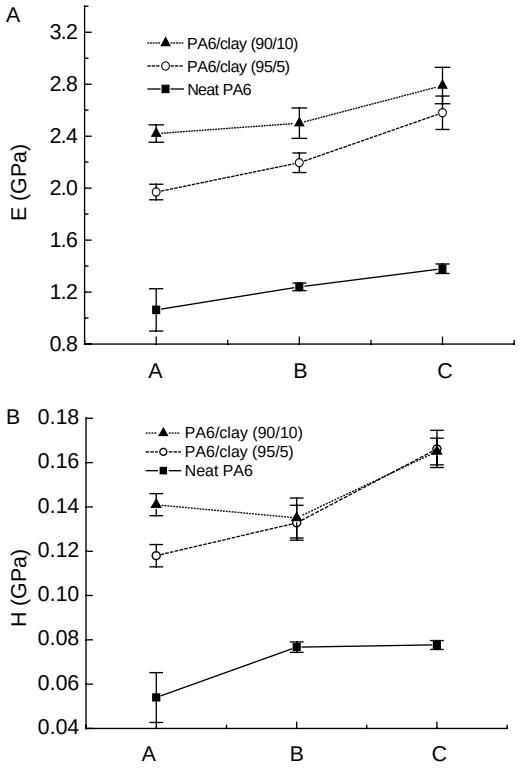

Fig. 9. Indentation measured modulus (A) and hardness (B) of surfaces (A, B and C) in the injection-molded bars for neat PA6 and its nanocomposites with 5 and 10 wt% clay.

the near-surface region, illustrating an uneven distribution of clay in the injection-molded sample, as also confirmed by optical microscopy [14]. That is, the content of clay increases from the sample surface to the inner region of the molded specimen. It is, therefore, expected that the inhomogeneous clay distribution in the injection-molded samples could lead to the different distribution of mechanical properties in the material.

Nanoindentation is used to detect the localized deformation behavior, and an attempt to study the mechanical properties at different locations in the injection-molded specimens of PA6 and the nanocomposites has been made. As shown in Fig. 1, the surfaces A, B and C represent the near-surface, intermediate, and core positions in the molding bar. The out-most layer, i.e. approximately 500 μm from the sample surface, is removed by polishing in order to exclude the uncertainties in top surface layer, such as roughness of the surface [44]. The indentation direction is normal to the A, B, C surfaces, i.e. perpendicular to the flow direction. Fig. 9(A) shows the variations of the modulus ($E_{\perp}$) perpendicular to the injection molding direction at the three planes for the neat PA6 and its nanocomposites with 5 and 10 wt% of clay. It can be seen that, compared to neat PA6, the modulus of the nanocomposite with 10 wt% clay increases by about 120% for all the three surfaces (A, B and C). For all samples, the modulus steadily increases from the surface to core (i.e. from A to B to C). The $E_{\perp}$ at surface A corresponds to the modulus reported in Fig. 3. For neat PA6, the modulus increases by about 17% from surface A to B and 11% from surface B to C. It is known that after molding,

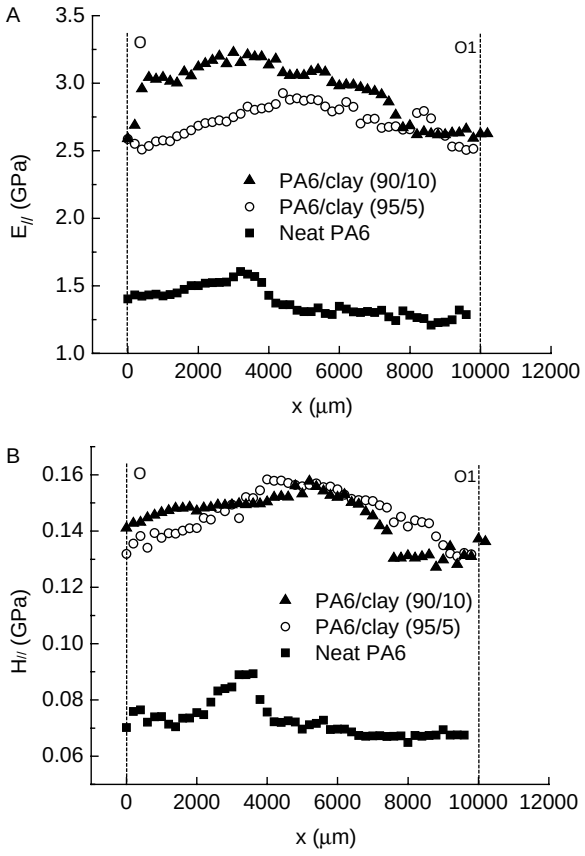

Fig. 10. Modulus (A) and hardness (B) profiles along the injection flow direction obtained from the measurements at the inner *xy* surfaces of injection-molded bars.

the outer part of the sample experiences a relatively faster cooling process (i.e. air-quenching) than the center, which usually leads to higher degree of crystallinity in the inner region than the outer [14]. This uneven distribution of crystalline morphology is believed to be the main reason of the enhancement in the modulus (from A to B to C) for the neat sample. For the case of the nanocomposites, it is worth to note that from surface B to C, the modulus enhancement is much prominent than that found in the neat sample. It is believed that addition of rigid clay is the main cause for this difference. As shown in Fig. 8(C) and the previous report [14], the clay distribution has relatively less density at the near surface region than in the core. Higher concentration of clay can lead to higher modulus in the core region.

The hardness ($H_{\perp}$) profiles of the three samples are shown in Fig. 9(B), showing similar phenomenon as observed in the modulus profile. The hardness of the nanocomposite with 10 wt% of clay is almost twice of the neat sample. Contrary to the others, the nanocomposite with 10 wt% of clay has insignificant difference between surface A and B. This could be related to the dispersion state of the clay nanofiller in the nanocomposite: exfoliated/intercalated mixture is usually observed at higher clay loading (e.g. >5 wt%) [14]. With clay loading further increases, clay agglomeration becomes evident which would result in higher chances for the indenter solely in contact with a clay cluster. Therefore, agglomeration could significantly affect the nanoindentation measurement when its size is comparable to the contact area.

Fig. 10(A) and (B) show the modulus ($E_{\|}$) and hardness ($H_{\|}$) fluctuation profiles along the x direction from point O to O_1 (refer to Fig. 1) in the plane of x–y for neat PA6 sample and the two nanocomposites. Clearly, both modulus and hardness of the nanocomposites are much higher (by about 100%) than those of neat PA6. Here the indentation direction is parallel to the injection direction. In this case, due to the effect of melt-processing, most polymer chains (as well as the clay platelets) approximately align along the indentation loading direction. For the neat sample, the difference in the mechanical properties may indicate variation of crystallinity at the corresponding localized area. It can be seen that along the line O–O_1, there is an outstanding peak (i.e. increase) at near center location for both modulus and hardness profiles. It clearly indicates that there is inhomogeneous distribution of the crystallinity from surface to core in the molded neat PA6 specimen, since different locations from the surface to core experience different cooling history upon injection. For example, the outer part of the molded bar is cooled rapidly like a 'quenching' process in the air. However, for the inner part in the sample, temperature gradient of the molded specimen leads to different crystallization rates as well as degree of crystallinity from surface to core. For the case of the nanocomposites, in addition to the effect of thermal history mentioned above, uneven distribution of clay (from surface to core) within the molded specimens

Table 1
Modulus (GPa) and hardness (GPa) of the PA6 and its clay nanocomposites in the directions of parallel (||) and perpendicular ($\perp$) to injection flow

	$E_{\|}$	$E_{\perp}$	$H_{\|}$	$H_{\perp}$
Neat PA6				
Surface (A)	1.16±0.01	1.06±0.16	0.085±0.001	0.054±0.011
Intermediate (B)	1.42±0.03	1.24±0.01	0.085±0.002	0.077±0.002
Core (C)	1.50±0.04	1.38±0.03	0.092±0.004	0.078±0.002
PA6/clay (95/5)				
Surface (A)	2.03±0.04	1.97±0.06	0.121±0.004	0.118±0.005
Intermediate (B)	2.37±0.04	2.20±0.08	0.142±0.001	0.133±0.008
Core (C)	2.96±0.13	2.58±0.06	0.173±0.004	0.166±0.008
PA6/clay (90/10)				
Surface (A)	2.63±0.11	2.42±0.07	0.150±0.011	0.141±0.005
Intermediate (B)	2.77±0.07	2.50±0.12	0.158±0.005	0.135±0.009
Core (C)	3.13±0.14	2.79±0.20	0.167±0.016	0.165±0.006

Table 2
Elastic modulus values from different measurements for PA6 and its nanocomposites as a function of clay loading

Clay loading (wt%)	$E_{\perp}$ (GPa) (from nanoindentation)	$E_{\parallel}$ (GPa) (from nanoindentation)	E (GPa) [41] (from tensile tests)
0	1.06±0.16	1.16±0.01	1.50±0.08
5	1.97±0.06	2.03±0.04	2.25±0.06
10	2.42±0.07	2.63±0.11	2.66±0.10

may play an additional role in affecting the modulus and hardness profiles. As shown in Fig. 10, instead of sharp peak in the core region on the hardness/modulus profiles for the neat sample, the increasing and decreasing amplitudes are much smooth and diffusing in the case of the nanocomposites, probably because the addition of clay nanofiller into the matrix dramatically reduces the crystal size of PA6 and thus may blur the crystallinity difference between the surface and core. However, the maximum values are still found in the core region as observed in the neat sample, mainly due to processing-induced gradient distribution of the clay platelets as well as the crystallinity difference resulted from temperature gradient (upon injection) from surface to core in the molded nanocomposites specimens [14].

Table 1 summarizes the hardness and modulus values of neat PA6 and the nanocomposites at the two indentation directions, i.e. parallel and perpendicular to the injection direction. As expected, all modulus and hardness in the direction parallel to the flow are higher than those obtained in the direction perpendicular to the injection direction. Thus, care should be taken when performing the mechanical measurements on the injection-molded semi-crystalline polymeric products since the different loading direction could generate different absolute values of modulus/hardness, especially for the particulate-filled multi-phase polymeric systems. Table 2 compares the moduli obtained from the indentation experiments and the tensile tests [45]. The modulus values (parallel to the injection flow) obtained by indentation are more comparable with the tensile results for the same systems. This is understandable since the loading direction for the tensile tests is also parallel to the flow direction. Moreover, the hardness and modulus on both directions increase monotonously from surface A to C, as shown in Table 1. The difference between local mechanical properties on surface and core regions can be as large as 20%.

4. Conclusions

In present study, nanoindentation has been used to probe the hardness, modulus, and creep behavior of the PA6/clay nanocomposites. Compared with the neat PA6 system, the modulus and hardness of the nanocomposites with 2.5 wt% of clay are enhanced by 74 and 80%, respectively. The values of the modulus and hardness keep on increasing with further increasing the nanoclay loading (e.g. here up to 10 wt%). With addition of clay, it is found that the crystal size and the crystalllinity of the PA6 matrix have been reduced significantly, as evidenced by TEM and X-ray measurements. It is believed that the creep resistance of the nanocomposite is not only enhanced by addition of the stiff clay platelets, but also deteriorated due to the reduced crystallinity and crystal size of the polymer matrix with addition of clay. The two competing effects are found to be balanced when the clay loading reaches 7.5 wt%. The nanoindentation also enables one to explore the mechanical anisotropy and the hardness/modulus distribution profiles resulted from the melt processing. The orientation of polymer chains and the distribution of clay platelets significantly affect the localized mechanical behavior of the nanocomposites. The hardness and modulus along the injection-molded flow direction are higher than those measured in the direction perpendicular to the melt flow. The nanoindentation results also prove that the core portion of the injection-molded specimens of PA6 and its nanocomposites generally possesses higher hardness and modulus than the outer part of the specimens, which is caused by the processing-induced uneven distribution of both crystallinity and nanoclay within the molded products.

References

[1] Okada A, Kawasumi M, Usuki A, Kojima Y, Kurauchi T, Kamigaito O. Mater Res Soc Proc 1990;171:45–50.
[2] Lan T, Pinnavaia TJ. Chem Mater 1994;6:2216–9.
[3] Zilg C, Muelhaupt R, Finter J. Macromol Chem Phys 1999;200:661–70.
[4] Pinnavaia TJ, Beall GW. Polymer-clay nanocomposites. NY, USA: Wiley; 2000.
[5] Giannelis EP. J Miner Met Mater Soc 1992;44:28–30.
[6] Kawasumi M, Kohzaki M, Kojima Y, Okada A, Kamigaito O. US Patent No. 4810734 1999 [assigned to Toyota Motor Co. Japan].
[7] Usuki A, Kojima Y, Kawasumi M, Okada A, Fukushima Y, Kurauch T, et al. J Mater Res 1993;8:1179–84.
[8] Okada A, Usuki A. Mater Sci Eng C 1995;3:109–15.
[9] Yano K, Usuki A, Okada A. J Polym Sci, Part A: Polym Chem 1997;35:2289–94.
[10] Kojima Y, Usuki A, Kawasumi M, Okada A, Fukushima Y, Kurauchi T, et al. J Mater Sci Lett 1993;8:1185–9.
[11] Kojima Y, Fukumori K, Usuki A, Okada A, Kurauchi T. J Mater Sci Lett 1993;12:889–90.
[12] Kojima Y, Usuki A, Kawasumi M, Okada A, Kurauch T, Kamigaito O. J Appl Polym Sci 1993;49:1259–64.
[13] Usuki A, Koiwai A, Kojima Y, Kawasumi M, Okada A, Kurauch T, et al. J Appl Polym Sci 1995;55:119–23.
[14] Liu TX, Tjiu WC, He CB, Na SS, Chung TS. Polym Int 2004;53:392–9.
[15] Xie SB, Zhang SM, Liu HJ, Chen GM, Feng M, Qin HL, et al. Polymer 2005;46:5417–27.
[16] Weon JI, Sue HJ. Polymer 2005;46 [available online 14 June].
[17] Yalcin B, Cakmak M. Polymer 2004;45:2691–710.
[18] Balta Calleja FJ, Privalko EG, Sukhorukov DI, Fainleib AM, Sergeeva LM, Shantalii TA, et al. Polymer 2000;41:4699–707.
[19] Azzurri F, Flores A, Alfonso GC, Sics I, Hsiao BS, Balta Calleja F. J Polymer 2003;44:1641–5.
[20] Balta Calleja FJ, Cagiao ME, Adhikari R, Michler GH. Polymer 2004;45:247–54.
[21] Krumova M, Flores A, Balta Calleja FJ, Fakirov S. Colloid Polym Sci 2002;280:591–8.
[22] Balta Calleja FJ, Fakirov S. Microhardness of Polymers. MA, USA: Cambridge University Press; 2000.
[23] Beake BD, Chen S, Hull JB, Gao F. J Nanosci Nanotech 2002;2:73–9.
[24] Oliver WC, Pharr GM. J Mater Res 1992;7:1564–83.
[25] Doerner MF, Nix WD. J Mater Res 1986;1:601–8.

[26] Baker SP, Weihs TP. Mater Res Soc Symp Proc 1993;308:217–9.
[27] Pharr GM, Oliver WC, Brotzen FR. J Mater Res 1992;7:613–7.
[28] Zhang WD, Shen L, Phang IY, Liu TX. Macromolecules 2004;37: 256–9.
[29] Liu TX, Phang IY, Shen L, Chow SY, Zhang WD. Macromolecules 2004; 37(7214):7222.
[30] Beake BD, Leggett GJ. Polymer 2002;43:319–27.
[31] Paiva A, Sheller N, Foster MD, Crosby AJ, Shull KR. Macromolecules 2001;34:2269–76.
[32] Pavoor PV, Bellare A, Strom A, Yang D, Cohen RE. Macromolecules 2004;37:4865–71.
[33] Liu TX, Mo ZS, Zhang HF, Li G. J Appl Polym Sci 1998;69:1829–35.
[34] Strobl GR, Schneider MJ. J Polym Sci, Polym Phys 1980;18:1343–60.
[35] Strobl GR, Schneider MJ, Voigt-Martin IG. J Polym Sci, Polym Phys 1980;18:1361.
[36] Askeland DR. The science and engineering of matierials. 3rd ed. London: Chapman & Hall; 1996.
[37] Lan T, Kaviratna PD, Pinnavaia TJ. Chem Mater 1995;7:2144–50.
[38] Liu TX, Kim KP, Tjiu WC, Parmoda KP, Chen ZK. Polymer 2003;44: 3529–35.
[39] Lincoln DM, Vaia RA, Wang ZG, Hsiao BS, Krishnamoorti R. Polymer 2001;42:9975–85.
[40] Lincoln DM, Vaia RA, Krishnamoorti R. Macromolecules 2004;37: 4554–61.
[41] Fornes TD, Paul DR. Polymer 2003;44:3945–61.
[42] Shen L, Phang IY, Chen L, Liu TX, Zeng KY. Polymer 2004;45:3341–9.
[43] Shen L, Phang IY, Liu TX, Zeng KY. Polymer 2004;45:8221–9.
[44] Shen L, Liu TX, Lv PF. Polym Test 2005; 24: 746–9.
[45] Liu TX, Liu ZH, Ma KX, Shen L, Zeng KY, He CB. Compos Sci Technol 2003;63:331–7.